QUARTERLY JOURNAL OF THE ROYAL METEOROLOGICAL SOCIETY
Q. J. R. Meteorol. Soc. (2008)
Published online in Wiley InterScience
(www.interscience.wiley.com) DOI: 10.1002/qj.349

Modulation of tropical convection by breaking Rossby waves

G. Allen,[a]* G. Vaughan,[a] D. Brunner,[b] P. T. May,[c] W. Heyes,[a] P. Minnis[d] and J. K. Ayers[d]

[a]*Centre for Atmospheric Science, University of Manchester, UK*
[b]*EMPA, Swiss Federal Institute for Materials Testing and Research, Dubendorf, Switzerland*
[c]*Centre for Australian Weather and Climate Research, Melbourne, Australia*
[d]*NASA Langley Research Center Science Directorate, Hampton, VA, USA*

ABSTRACT: This work discusses observations of both the convective-inhibiting and convective-promoting properties associated with Rossby waves that break in the extratropics and extend into the tropics. Two tropical drought periods – times of reduced tropical cloudiness and rainfall – were observed during mid to late November 2005 over a wide area of north-west Australia, with an observed eruption of a nearby synoptic tropical cloud band in between times. Both convective inhibition and promotion appear to be linked to the descent of dry upper tropospheric air within a series of tropopause folds; convective inhibition was observed within the dry pool itself, whilst convective promotion was observed on the high moisture gradient at the leading edge of an advancing dry slot. A range of satellite images, surface rain gauges, radiosonde and ozonesonde data are used in conjunction with back trajectories and European Centre for Medium-Range Weather Forecasts (ECMWF) analysis fields to investigate the origins and dynamics associated with these convective events, showing each to be ultimately linked to breaking Rossby wave activity on the southern subtropical jet. Together, these observations support a growing number of studies linking midlatitude tropopause-level dynamics with the modulation of tropical deep convection, an influence that is poorly characterized when considering the climatology of tropical cloudiness and rainfall.

KEY WORDS convection; tropopause fold; Rossby waves; stratosphere to troposphere exchange

Received 28 April 2008; Revised 2 October 2008; Accepted 24 October 2008

1. Introduction

Breaking Rossby waves and associated tropopause folds are ubiquitous features of upper tropospheric meteorology and are reasonably well understood theoretically (Hoskins and Ambrizzi, 1993). The distribution of stratospheric tracers in and around tropopause folds was first described by Danielsen (1968) and has been confirmed by many subsequent studies. Less well understood is the influence of folds on lower level dynamics, specifically their ability to modulate convection. Previous case studies of convective modulation by upper level PV anomalies have reported both convective destabilization and convective inhibition under different circumstances (see below).

Deep convection in the tropics is one of the main engines of the general circulation and is one of the most difficult processes to represent correctly in general circulation models. A thorough understanding of the large-scale influences on tropical convection is therefore a prerequisite for successful modelling of the atmosphere. In this paper we examine the role of breaking Rossby waves generated along the Southern Hemisphere (SH) subtropical jet stream (STJ), but in their final form extending well into the tropics, on the distribution of deep convection over north-west Australia. These waves generate characteristically filamentary structures in the horizontal, taking the form of tropopause folds in the vertical dimension. The contrasting mechanistic effects of folds on convection are now discussed briefly.

1.1. Convective inhibition

Folds can extend well down into the troposphere, setting up deep dry layers of enhanced static stability, which act as lids on any upwelling convection.

The radiative dynamic implications of dry layers (or tongues) in the tropical maritime troposphere were discussed by Mapes and Zuidema (1996) and Parsons (1999) using measurements made during the Tropical Ocean Global Atmosphere Coupled Ocean Atmosphere Response Experiment (TOGA-COARE) field campaign centred on the Solomon Islands. Although not attributed directly to tropopause folding, they showed that commonly observed dry layers over the tropical western Pacific (TWP) advected from the subtropical upper troposphere were correlated with periods of reduced precipitation and reduced occurrence of deep convection – termed a 'tropical drought'. The entrainment of dry air in the free troposphere was cited as a likely cause of convective suppression, coupled with strong radiatively induced thermal inversions as a result of the high gradient in water vapour concentration at the bottom of such dry layers, an effect

**Correspondence to: G. Allen, Centre for Atmospheric Science, University of Manchester, Oxford Road, Manchester, M13 9PL, UK.
E-mail: grant.allen@manchester.ac.uk

noted by Cau *et al.* (2005). Further analysis of the origins of dry layers over the TWP by Yoneyama and Parsons (1999) showed that dry air advected to the TWP was transported in baroclinic waves of Northern Hemisphere (NH) subtropical origin and in one case by a breaking Rossby wave on the SH STJ. A later, more detailed case study of a dry-tongue event during TOGA-COARE by Parsons *et al.* (2000), albeit limited to the maritime troposphere, again showed a marked and correlated reduction in rainfall and convective activity, and reported that radiatively induced convective inhibition (CIN) alone may, unusually, be enough to suppress convection in the TWP. However, they highlighted the need for further studies of this type to confirm such findings and noted the need for a correction to their radiosonde data set, not available at that time.

1.2. Convective promotion

Conversely to the above, if such dry layers overrun layers of moist boundary layer air, convection may result if sufficient forcing is available to release the potential instability generated by the layers. The ability of tropopause folds to promote deep convection through potential instability was recognized as far back as Danielsen (1968), and there have been a number of studies in the literature of this phenomenon (Browning and Roberts, 1994; 1995; Morcrette *et al.* 2007). By this mechanism, a tropopause fold generates regions of potential instability when dry layers inherent to folds overlay layers of moist air at lower levels, thus leading to a decreasing wet-bulb potential temperature profile with height. The release of this potential instability (through convection) requires sufficient forced ascent of the lower layer; for example by topographic forcing, as noted by Roca *et al.* (2005), or sea-breeze convergence. However, such forcing is not always present and therefore the potential instability generated by tropopause folds is not always realized.

Several other studies have linked Rossby wave propagation into the tropics with the promotion of deep convection (Slingo, 1998; Kiladis, 1998; Yoneyama and Parsons, 1999; Knippertz, 2005). So-called tropical plumes (TPs), or south-west–north-east orientated (in the NH) synoptic-scale cloud bands stretching from the tropics to the subtropics (or even the midlatitudes), have been found to coincide with mobile upper-level troughs (Knippertz and Martin, 2006); such troughs take the form of elongated stratospheric potential vorticity (PV) streamers or cut-offs linked to the crests of breaking Rossby waves. However, as noted by Knippertz (2007), there is some question in the literature regarding the physical processes involved in the relationship between TPs and upper-level troughs at low latitude, the key issue being whether the observed lifting is a result of dynamical forcing, convective heating or some interaction of the two.

1.3. Structure of this study

In this paper, we examine two tropical drought periods, separated by a period of enhanced convective activity and tropical cloudiness, which occurred over north-west Australia in November 2005 (during the wet season), and relate these events to the passage of breaking Rossby waves and associated tropopause folds. The study compares ozonesonde, radiosonde and surface rain gauge data with satellite-derived cloud information and imagery, and European Centre for Medium-Range Weather Forecasts (ECMWF) analyses. We will focus on the second of these two drought periods in greater depth, examining the prevailing dynamics and the transport of dry air masses. We will also discuss the meteorological influences on the period of increased tropical cloudiness between the two drought periods. In this case study we hope to illustrate more clearly the different mechanisms by which tropopause folds can modulate tropical convection.

2. Data and methodology

For the purposes of this case study, we confine our analysis to the one-month period between 10 November 2005 and 10 December 2005, to make full use of the intensive observation period of the UK Aerosol and Chemical Transport in tropical conVEction (ACTIVE) aircraft campaign, conducted from Darwin, Australia (12.46°S, 130.93°E). The ACTIVE campaign and ozonesonde and meteorological data discussed herein are described further by Vaughan *et al.* (2008). This campaign was conducted during the 2005/2006 wet season (November–February) from Darwin, Australia, as part of an extensive field campaign to study tropical convection and its effect on the tropical tropopause layer, in tandem with the Stratospheric-Climate Links with Emphasis on the Upper Troposphere and Lower Stratosphere (SCOUT-O3) campaign (also described by Vaughan *et al.* 2008).

For the purposes of this study, a region of interest (herein referred to as the ROI) over tropical north-west Australia is defined between 120°E–133°E and 12°S–20°S, based on MTSAT-1R satellite observations of a prevalent dry slot during the drought period. The ROI is indicated by the diagonally hatched area in Figure 1; the dry tongue over the ROI is seen as a dark area in the water vapour field.

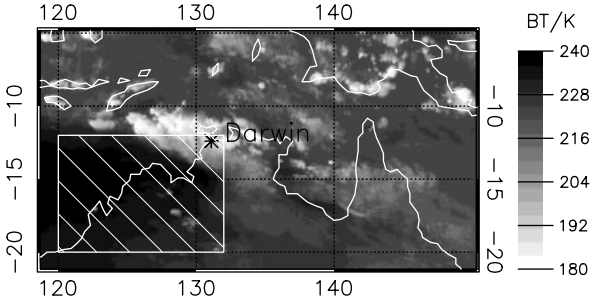

Figure 1. Grey-scale image of MTSAT-1R water-vapour channel brightness temperatures over northern Australia at 0530 UTC on 20 November 2005, showing a cloud plume over Darwin. The cross-hatched area defines the ROI. Dark areas indicate dry air at mid-levels.

DOI: 10.1002/qj

2.1. Vertical soundings from Darwin

During November 2005, Vaisala RS80 radiosondes were launched twice daily at 1100 UTC (2030 local) and 2300 UTC (0830 local) from Darwin Airport by the Australian Bureau of Meteorology (BoM). Pressure, humidity, wind and temperature data were recorded every 10 seconds during ascent, giving a vertical resolution of roughly 20 m on average in the troposphere. On days of scientific interest to ACTIVE or SCOUT-O3, electrochemical concentration cell ozonesondes were added to the radiosonde payload and a Vaisala RS92-KE sonde was used instead of the RS80. Following Reid *et al.* (1996), we applied a constant background current correction to the ozonesonde measurements in the troposphere, rather than the standard pressure-varying correction. Measured ozonesonde profiles were consistent (± 5 ppbv) with ozone profiles recorded by the SCOUT-O3 Geophysica aircraft. A total of 29 such ozonesondes were launched from Darwin airport during the ACTIVE campaign, with five available during the drought period of interest to this study.

2.2. ECMWF analyses

Wind, pressure, temperature, specific humidity and vertical motion fields used here were taken from data hosted by the British Atmospheric Data Centre (BADC) and produced by the ECMWF operational analysis Integrated Forecasting System (IFS Cycle 29r2). The above fields were provided on a $1.125^\circ \times 1.125^\circ$ grid on 60 hybrid model levels. Isentropic fields of these variables were constructed by interpolation between model levels. Isentropic PV fields were calculated by linearly interpolating winds and static stability on to isentropic surfaces, then calculating PV from these fields.

2.3. Satellite data

The Japanese Meteorological Agency Multi-functional Transport Satellite (MTSAT-1R), launched on 26 February 2005, is a geostationary satellite providing coverage for the hemisphere centred on 140°E. It provides imagery in five wavelength bands: one visible (0.55–0.80 μm), two infrared (10.3–11.3 μm; 11.5–12.5 μm), one near-infrared (3.5–4.0 μm) and a further infrared channel sensitive to water vapour (6.5–7.0 μm). The visible and infrared cameras have spatial resolutions of 1 and 4 km at the nadir point respectively (resolution is lower away from the equator and at 140°E). A portion of an MTSAT-1R water vapour channel image is shown in Figure 1.

Cloud data products used in this study were retrieved from MTSAT-1R imagery (described further by Minnis *et al.*, 2006) using the Visible Infrared Solar-Infrared Split Window Technique (VISST) and the Solar-Infrared Infrared Split Window Technique (SIST) method of Minnis *et al.* (1995). This method uses MTSAT-1R brightness temperatures in all channels during daytime (VISST) and night-time (SIST), in conjunction with other available satellite and meteorological observations, to derive information on cloud-top height, cloud phase, cloud thickness and other parameters.

2.4. Surface rain-gauges

This tropical location also benefits from the presence of a comprehensive rain gauge network operated by the Australian BoM across north-west Australia and the Northern Territory. The region of interest discussed in this work contains a total of 643 rain gauges read daily at 2330 UTC (0900 local time). This study uses a $0.5^\circ \times 0.5^\circ$ gridded rainfall product derived from all available rain gauges, provided by the BoM.

2.5. Tropopause fold definition

Tropopause folds have been extensively described in the scientific literature as layers of ozone-rich dry air with PV extending downwards and equatorwards beneath jet streams (Danielsen, 1968). In mid and high latitudes, in the vicinity of a jet stream, folds may be identified by potential vorticity alone and therefore identified from standard weather analysis fields (Sprenger *et al.*, 2003), although complex algorithms relying on the spatial morphology of the features are generally required, rather than simple PV thresholds. In addition, as folds move away from the jet stream, the dynamical signature of high PV disappears more quickly than the chemical signature of elevated ozone and low humidity. Bithell *et al.* (2000) examined a case where a dry layer with elevated ozone but no static stability anomaly could be tracked back to a tropopause fold beneath the polar jet stream around 10 days previously. The PV was presumed to have decayed by radiation, consistent with the calculation of Forster and Wirth (2000). At low latitudes, values of 2 PV units (1 PVU = 1026 K m^2 s^{-1} kg^{-1}), used more generally to denote the dynamical tropopause in the extratropics, do not capture structures with the morphology of tropopause folds, and it is necessary to use lower PV thresholds to identify them. In this work, based on examination of PV fields, comparison with ozonesondes and use of trajectory analysis to confirm air mass origin, we consider regions where the magnitude of PV exceeds 0.5 PVU to be chemically influenced by stratospheric air. As in Sprenger *et al.* (2003), we use the morphology of the folds as well as the PV values to identify them.

3. Meteorological context

The wet season in northern Australia typically starts in October with the pre-monsoon 'build-up' period characterized by weak easterly trade winds at low levels and a strong diurnal evolution of isolated storms and mesoscale systems typical of continental tropical convection. A more detailed description of the regional meteorology during the ACTIVE and SCOUT-O3 campaigns is given by Brunner *et al.* (2008). Throughout early to mid November 2005, typical pre-monsoon conditions were observed over the ROI, with local sea-breeze circulations generating a range of convective storms, from isolated thunderstorms to squall line complexes ~ 100 km in scale. Such deep convective storm systems regularly

DOI: 10.1002/qj

achieved cloud-top heights in excess of 18 km (Vaughan *et al.*, 2008).

Winds near Darwin showed the normal pattern of land–sea breeze circulation, with generally easterly winds in the morning turning to westerly in the afternoon. An exception to this general pattern occurred during 19–23 November, when the convective steering level wind direction switched from the prevailing easterlies to a deep westerly flow from 700–200 hPa, associated with an extensive region of convection over the ocean, west of Top End of Australia. This event was the tropical cloud band discussed in detail below.

4. Discussion: observations of a drought over northern Australia

Here, we will discuss the broad pattern of convection during two drought periods over the ROI during November 2005, focusing on the latter of the two drought periods in the context of a case study, before discussing observations of a tropical cloud band to the north of the ROI, which occurred between these two dry periods.

4.1. Convective characteristics over the ROI

During two periods between 16–19 November 2005 and 23–27 November 2005, much reduced cloud cover and precipitation was observed over the ROI. A time sequence of satellite-observed fractional cloud cover over the ROI, together with area-averaged ECMWF-derived PV and vertical motion evaluated at 325 K potential temperature (mid-troposphere) is plotted in Figure 2(a); 325 K was chosen as a representative level with the mid-tropospheric dry layer over the ROI. The corresponding time series of daily accumulated surface rain-gauge data averaged over the ROI, together with ECMWF forecast rainfall and ECMWF relative humidity (RH) evaluated at 325 K is plotted in Figure 2(b). Together, Figure 2(a) and (b) show a marked reduction in measured rainfall over the area during these two periods, herein referred to as drought periods 1 and 2, or DP1 and DP2, respectively.

The beginning of both drought periods was marked by peaks in both PV and positive ω (vertical motion in pressure coordinates), indicating large-scale subsidence. Note that the modulus of PV is used herein, but that PV is negative by convention in the SH. During DP2, cloud cover is also seen to be much reduced ($<2\%$ over the ROI). Conversely, cloud cover appeared to remain fairly constant during DP1, although in general such cloud appears to be non-precipitating based on rain gauge data. On closer inspection of MTSAT-1R Channel 1 brightness temperatures, we note that much of the cloud observed during DP1 was found at high levels (low brightness temperature) and advected from deep convective systems upstream of the ROI.

It is interesting to note that in each of the two dry periods, rainfall remained low even after the area-averaged PV signature returned to baseline values, suggesting that convection was being inhibited by the dry air remaining after the PV signature had decayed. It is also noteworthy that measured rainfall through most of November is greatly in excess of that predicted by ECMWF analyses, in contrast to December when the two are similar. Evidently, the ECMWF rainfall parametrization scheme did not work correctly in the early part of the build-up season.

A sequence of cloud-top height (CTH) maps derived from MTSAT-1R brightness temperatures over the ROI is shown in Figure 3, illustrating the vigour of convective activity in the area before, during and after DP2. In each case, CTH observations are shown at 3 pm local time (0530 UTC), the approximate time of peak convective activity. Before DP1, in the typical case of 14 November (Figure 3(a)), there is widespread convection along the coast and inland, with CTH reaching in excess of 16 km. However, during DP2 (Figure 3(b)) we see greatly reduced convective activity over the area, with the remaining convection confined to coastal regions, where strong sea-breeze convergence is found, with slightly lower cloud heights of 14 km at maximum. A return to typical wet season convection occurs on 28 November (Figure 3(c)) with widespread land and coastal cells.

This picture of reduced cloudiness and rainfall during periods of large-scale descent and low mid-level humidity is not surprising. However, the high PV associated with the descending air mass seen here indicates a tropopause-level origin (as we shall discuss in the following section) and hence isentropic transport from higher latitudes, which has not previously been associated with tropical droughts.

4.2. Upper level dynamics affecting the ROI during DP2

Potential vorticity and wind vector maps derived from ECMWF analyses are plotted in Figure 4 for the 335 K isentrope (approximately 360 hPa over Darwin), showing a time evolution of these fields in the upper troposphere over the Indian Ocean and Australia during DP2. Note that 335 K better depicts the structure of the breaking Rossby wave compared with the 325 K level used in the previous section to represent the mid-tropospheric dry layer. On 20 November, a breaking Rossby wave on the STJ, seen as the westward pointing red protrusion in Figure 4(a)), developed over south-west Australia. By 22 November, the wave crest had moved eastward, with evidence of two breaking events on the STJ, seen as two closely spaced wave crests in Figure 4(b). A streamer of high PV extended westward over the ROI from the first wave peak. By 23 November the second of the two breaking waves extended toward the north with a near north–south orientation (Figure 4(c)) and moved eastward across the ROI. The greater penetration of this wave to lower latitudes appears to have been assisted by the westerly momentum imparted at lower latitudes by the preceding breaking event, evident as the strong westerly winds seen at 20 °S, 130 °E in Figure 4(b). Such facilitation is consistent with the

DOI: 10.1002/qj

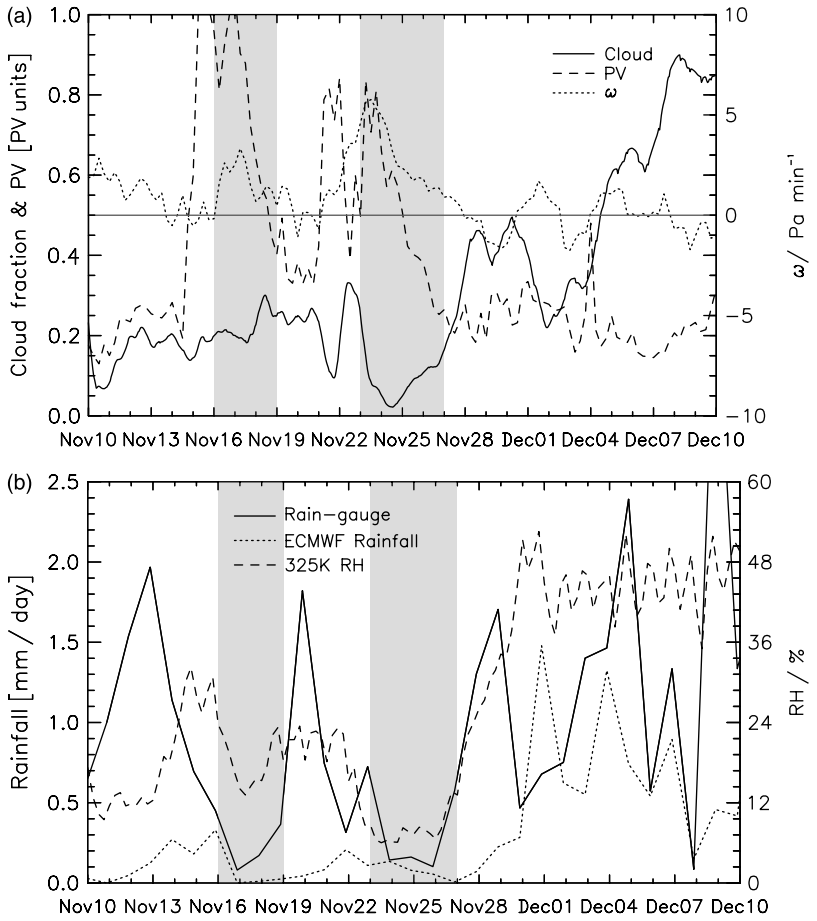

Figure 2. Time series of (a) fractional area of the ROI covered by cloud inferred from MTSAT-1R imagery, with area averages of ECMWF-derived potential vorticity (absolute value, in PV units) and vertical motion (ω) on the 325 K isentrope; (b) accumulated daily rainfall measured by surface rain gauges with area-averaged ECMWF surface rainfall and relative humidity (RH) on the 325 K isentrope. Shaded areas show two drought periods (see text for details).

findings of Davidson *et al.* (2007) and earlier studies, which show that wave propagation is favourable in an embedded westerly flow. Furthermore, an upper level anticyclone is observed upstream of the PV trough to the west (Figure 4(c)), which acted to stretch a streamer of high PV over the ROI extending from the breaking wave. By 25 November, this upper level anticyclone (upper level ridge) had moved over the ROI marking an area of large-scale downward motion, while the STJ had retreated southward (Figure 4(d)), leaving residual PV $\sim$ 0.7 PVU over much of the ROI. A quiescent STJ was re-established to the south on 27 November (Figure 4(e)).

Vertical cross-sections of PV, RH and potential temperature through the 125°E meridian (centre of the ROI) are plotted in Figure 5 and reveal the vertical structure of the tropopause fold associated with the double breaking event as it passed over the ROI during DP2, seen as a finger of very dry, high PV air which protrudes from the STJ. The 335 K isentrope can be used to relate fields plotted in Figure 5 to those plotted in Figure 4. Before the crest of the Rossby wave crossed this meridian on 20 November (Figure 5(a)), the STJ lay south of the ROI. On 22 November (Figure 5(b)) the elongated PV streamer associated with the first wave of the double-breaking event (Figure 4(b)) is observed at 15°S, with the spatially separated fold of the second breaking event seen at 18°S. On 23 November a second tropopause fold descended from upper levels beneath the STJ (Figure 5(c)). This fold gradually diminished in prominence over the next two days, before a quiescent (no Rossby wave activity) jet stream was seen to the south on 27 November (Figure 5(e)).

The dry air transported from the upper troposphere within these folds continued to be evident over the ROI well after the PV signature had been lost to diabatic processes. A pool of very dry (less than 10% RH) air resided over the ROI for the period 23–27 November, correlated with the period of reduced cloud cover and precipitation shown in Figure 2.

4.3. Vertical soundings and back trajectories

Ozonesondes launched from Darwin Airport during the passage of the fold (Figure 6) showed very dry layers with enhanced ozone concentration in the mid-troposphere. Such high ozone concentrations and anticorrelated water vapour are characteristic of tropopause folds. At 0500 UTC (1430 local) on 22 November at Darwin (Figure 6(a)), a layer of enhanced ozone (up to 130 ppbv)

DOI: 10.1002/qj

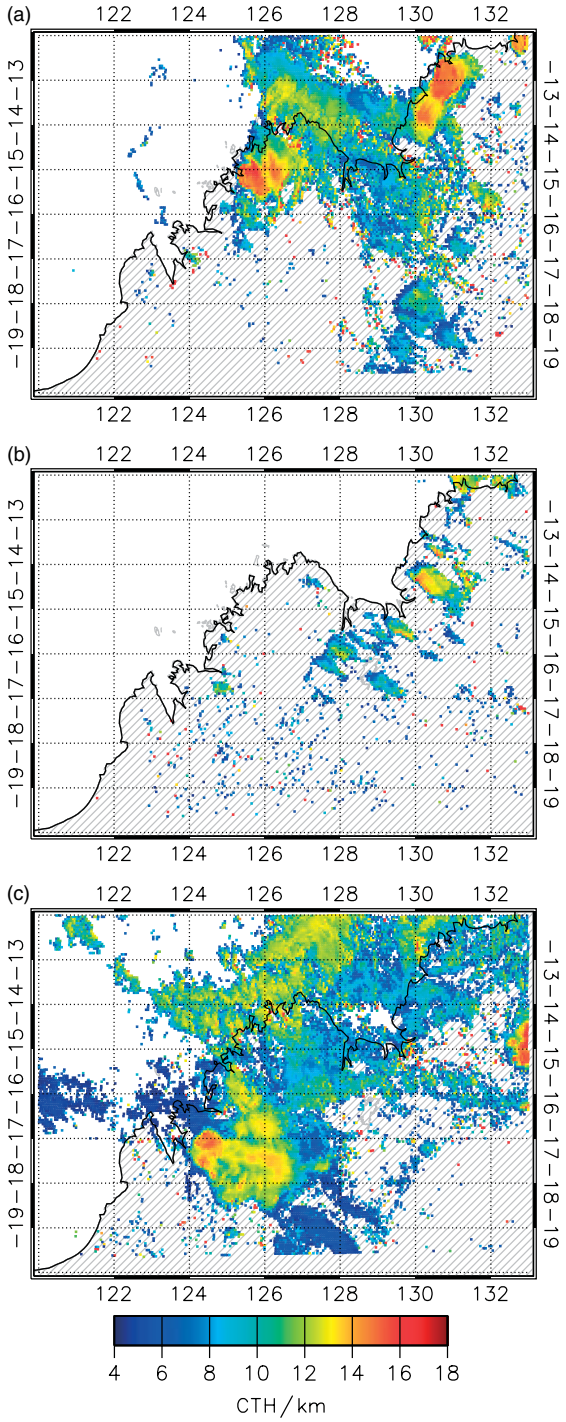

Figure 3. Cloud-top heights (km) derived from MTSAT-1R infrared brightness temperatures within the region of interest at 0556 UTC (1456 local time) on (a) 14 November 2005, (b) 23 November 2005 and (c) 28 November 2005.

and reduced RH (<10%), was observed between 390 hPa and 530 hPa or 336 K and 322 K potential temperature, respectively. Comparing this with Figures 4(b) and 5(b), we see that this layer is associated with the first of the breaking waves on a day when rainfall and cloud cover were reduced over the ROI (recall Figure 2). On 23 November (Figure 6(b)), there were thin layers of enhanced water vapour and reduced ozone in the mid-levels, characteristic of localized shallow convective uplift and outflow, with another thin layer of ozone-rich dry air at 350 mb (338 K) that also had high static stability (not shown). On 24 November (Figure 6(c)), the convective signature was absent but a pronounced very dry layer (<10% between 430 mb [262 K] and 520 mb [325 K]) was observed, coincident with increases in ozone up to almost 100 ppbv. This dry layer deepened and thickened by 27 November (Figure 6(d)), before a return to a more climatological humidity and ozone profile on 30 November (Figure 6(e)), with convective detrainment layers once more evident in the measured profile. Figure 7 shows four-day, three-dimensional back trajectories ending at 500 mb in a cluster around 12.4°S, 130.9°E (Darwin) at times corresponding to the ozonesonde profiles in Figure 6. The three profiles with enhanced ozone layers (22, 24 and 27 November) show little dispersion within the trajectory clusters, allowing an estimate of air parcel origin. On 22 November, when the highest ozone concentration during this period was measured (130 ppbv), four of the five trajectories originated from the PV filament extending westward from the breaking Rossby wave. On 27 November the cluster originated from the tip of the PV streamer, wrapping anticlockwise around the upper level anticyclone west of Australia, while on 24 November the cluster originated from the northern edge of the jet stream around 30°S, 100°E. On 23 November, the cluster diverges – two trajectories originate from the stratosphere and the other three remain in the troposphere ahead of the breaking Rossby wave. Divergence of the cluster means the air parcel origin cannot be inferred for this day. Finally, on 30 November, when the profile is again free of ozone-rich dry layers, the cluster remains in the troposphere with no connection to a PV filament (Figure 7(e)). This analysis is consistent with a stratospheric origin for the layers on 22 and 27 November, and a tropospheric origin on 30 November. For the 24 November the cluster originated north of the STJ in a region of PV in the range 0.4–0.7 PVU. This range is similar to that at the trajectory end points on 22 and 27 November, confirming the point made above that air with a clear chemical signature corresponded to absolute PV values much lower than 2 PVU. However, on 22 and 23 November, ozone-rich dry layers plotted in Figure 6(a) and (b) respectively coincided with high static stability, suggesting high PV (although PV cannot be derived from a single thermodynamic profile). One possible reason for the relatively low PV air (0.4 PVU) at the trajectory origin observed in the ECMWF analyses plotted in Figure 7(a) may be the inability of the ECMWF model to resolve vertically thin layers such as those evident in the radiosonde profile plotted in Figure 6(a). However, on 24 and 27 November static stability was not enhanced in radiosonde data, suggesting a genuine diabatic loss of potential vorticity consistent with the conclusion of Bithell *et al.* (2000), discussed earlier in section 2.5, that layers of stratospheric air entrained into the troposphere retain their chemical signature far longer than their enhanced PV (or static stability).

DOI: 10.1002/qj

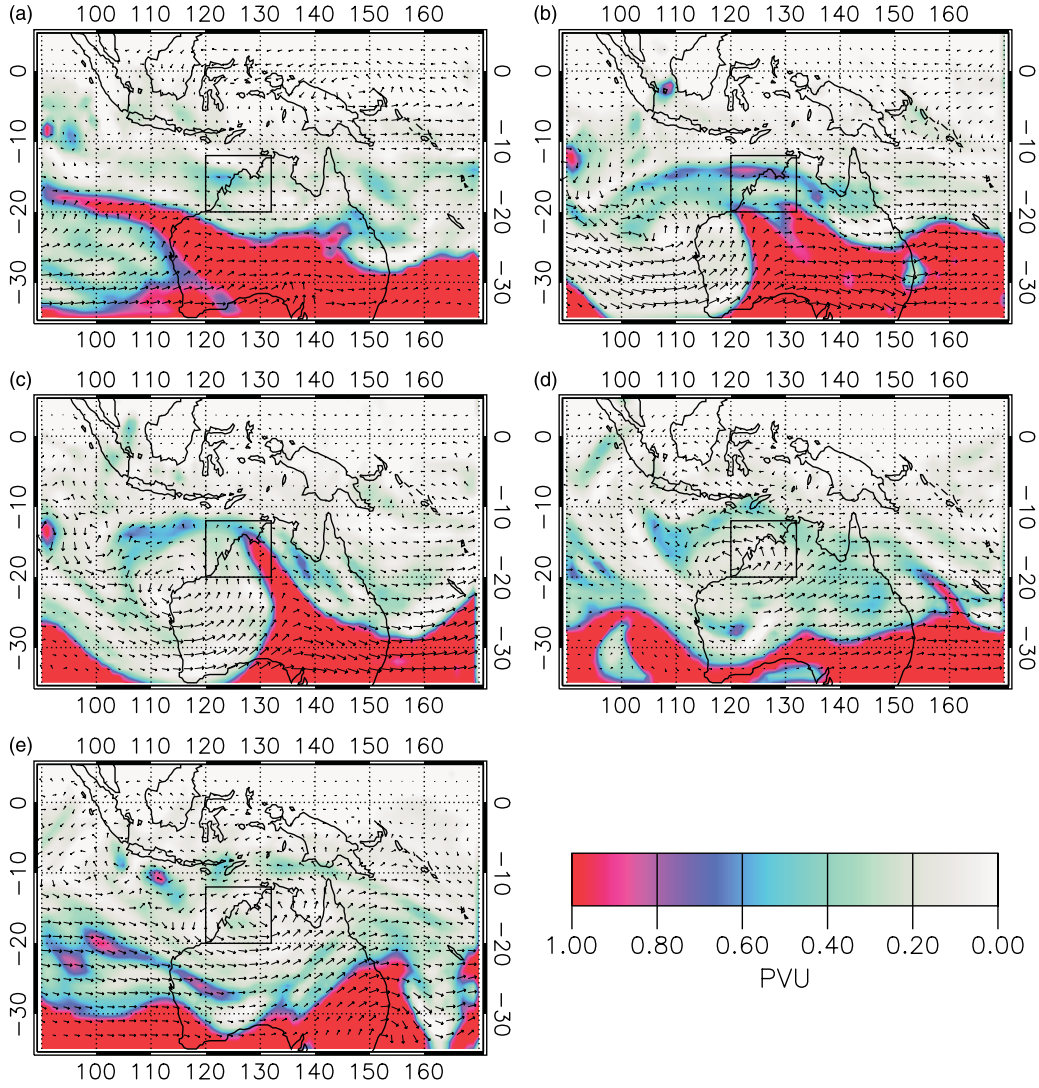

Figure 4. Isentropic (335 K) potential vorticity (colour contours) and wind fields (arrows) derived from ECMWF analyses over the Australian synoptic area for (a) 20 November 2005 1200 UTC, (b) 22 November 2005 1200 UTC, (c) 23 November 2005 1200 UTC, (d) 25 November 2005 1200 UTC and (e) 27 November 2005 1800 UTC. The solid blue contour indicates the −2 PVU surface. The black box defines the ROI.

5. Discussion: observations of a tropical cloud band

In the period between DP1 and DP2 (20–22 November), an eruption of convective activity occurred to the north of the ROI, predominantly over the Arafura Sea to the west of Darwin. A time sequence of the first of these convective events is plotted in Figure 8, which shows false-colour water vapour channel images recorded by MTSAT-1R. Convection was initiated at 2226 UTC on 19 November (0756 local time on 20 November) on the western coast of Australia at 129.5°E, 15.6°S (seen as the blue points at 130°E, −15°S in Figure 8(a)), seen as isolated bright white points. These initially isolated convective cells were observed within an eastward advancing dry slot (seen as the dark area in Figure 8(a)). The fact that this convection occurred only shortly after local sunrise, and over the sea, shows that it was not forced by solar heating of the continental boundary layer and suggests a dynamically forced release of potential instability.

Figure 8(b)–(h), recorded at one-hourly intervals, show the rapid development of a line of deep convection spreading to the north and west from the initial point on the coast, near the boundary between the moist and dry air masses. Over a period of six hours, this convective line developed to span 6° of longitude across tropical latitudes.

The rapid development of this line over such a large distance rules out self-propagation (by gust-front forcing for example) – the required phase speed would be of the order of 40 m s^{-1} and therefore too high for such processes. Furthermore, Figure 8(f) and (g) shows isolated development of convective cells to the north-east of the main plume along the moist–dry boundary, which later became part of the plume (Figure 8(h)). These isolated cells further suggest that the convective line was not dynamically linked to the initial convection, but does demonstrate a causal link associated with the dry–moist air mass boundary. This link is investigated further in Section 5.3.

DOI: 10.1002/qj

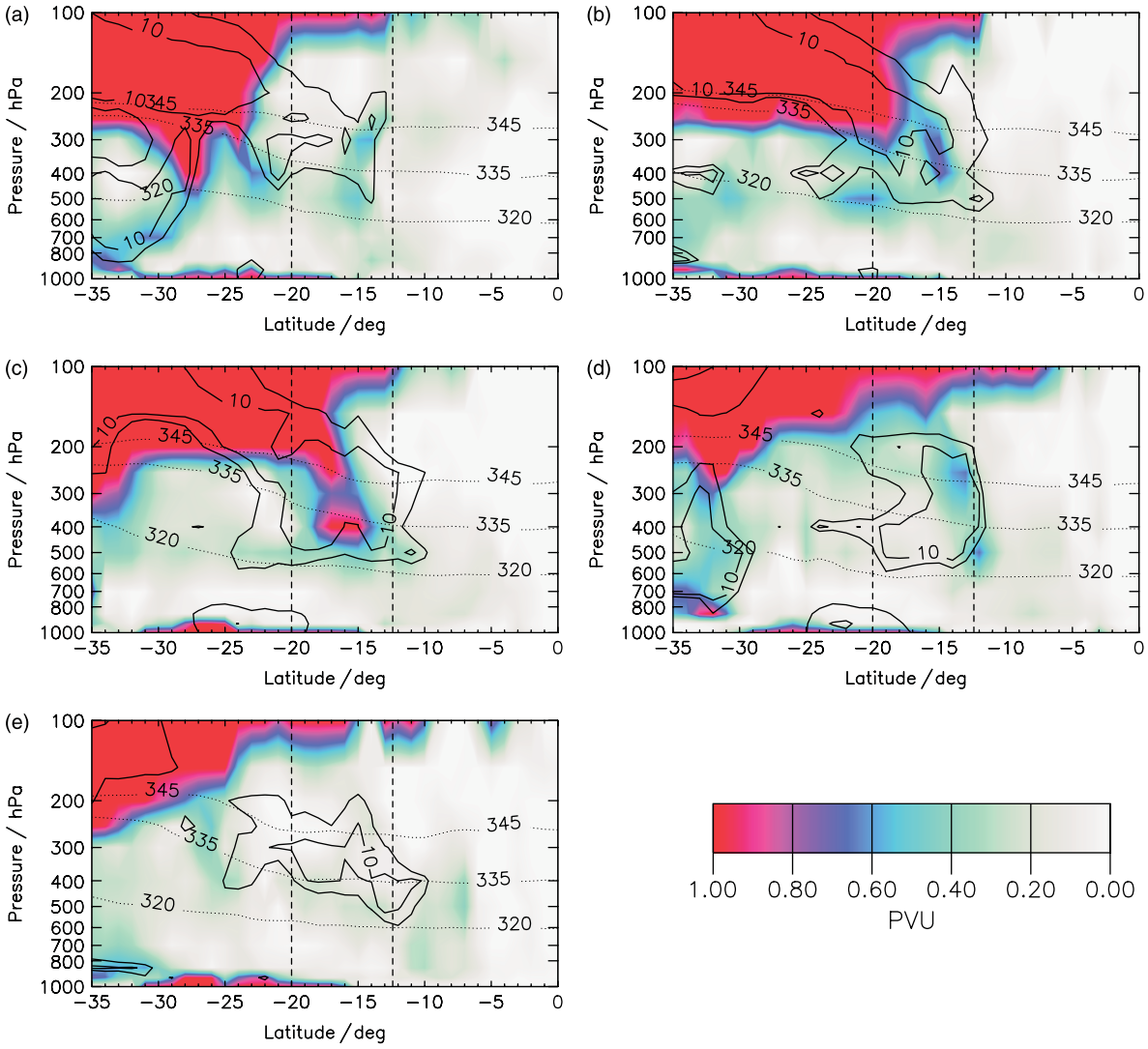

Figure 5. Vertical latitudinal cross-sections through the 125°E meridian of PV (colour contours), the 10% and 20% RH area (solid black contours) and potential temperature surfaces at 320, 335 and 345 *K* (dotted contours) for (a) 20 November 2005 1200 UTC, (b) 22 November 2005 1200 UTC, (c) 23 November 2005 1200 UTC, (d) 25 November 2005 1200 UTC and (e) 27 November 2005 1800 UTC. Dashed vertical lines indicate the latitudinal bounds of the ROI.

5.1. Thermodynamics of the plume

Figure 9 shows convective available potential energy (CAPE) and CIN, derived here for surface air from ECMWF thermodynamic profiles on 60 model levels at 0000 UTC (0930 local time) on 20 November 2005, corresponding to the satellite image in Figure 8(c). We see, from Figure 9(a), that there is a region of high CAPE to the north and east of the convective line observed in Figure 8 and a region of very low CAPE to the south and west. This region of low CAPE over the ocean to the south-west of the plume is coincident with a region of high CIN (up to 400 J kg^{-1}), coinciding with the eastward advancing dry slot seen in the satellite images of Figure 8. Hence, we see that the observed convective plume was initiated within a region of low convective inhibition (less than 100 J kg^{-1}) and significant CAPE (∼2000 J kg^{-1}) on the leading edge of the advancing dry slot. It is also noteworthy that CIN was very low (<50 J kg^{-1}) and CAPE very high over the northern tip of Australia at this time, but deep convection was not initiated there. We now investigate the factors that led to the eruption of convection at the leading edge of the dry slot.

Figure 10 shows a vertical-latitude cross-section of wet-bulb potential temperature (θ_w) and RH, calculated from ECMWF thermodynamic fields, through the 129°E meridian at 0000 UTC (0930 local time) on 20 November 2005, again corresponding to the satellite image in Figure 8(c). This represents a cross-section through the tropical cloud band, near the point of coastal initiation in Figure 8(a). The white dashed line marks the point where convection was seen to be initiated in Figure 8(a). Three salient features may be identified in this figure: (1) the moist boundary layer with ($\theta_w > 296$ K), (2) the very dry region above 500 mb and south of 14° latitude, corresponding to the dry slot in the satellite water vapour image, and (3) the two regions of potential instability (minima in θ_w), one at the base of the dry layer at 500 mb and the other a much smaller feature at 900 mb, between 16°S and 12°S. It is the lower level feature – not the one

DOI: 10.1002/qj

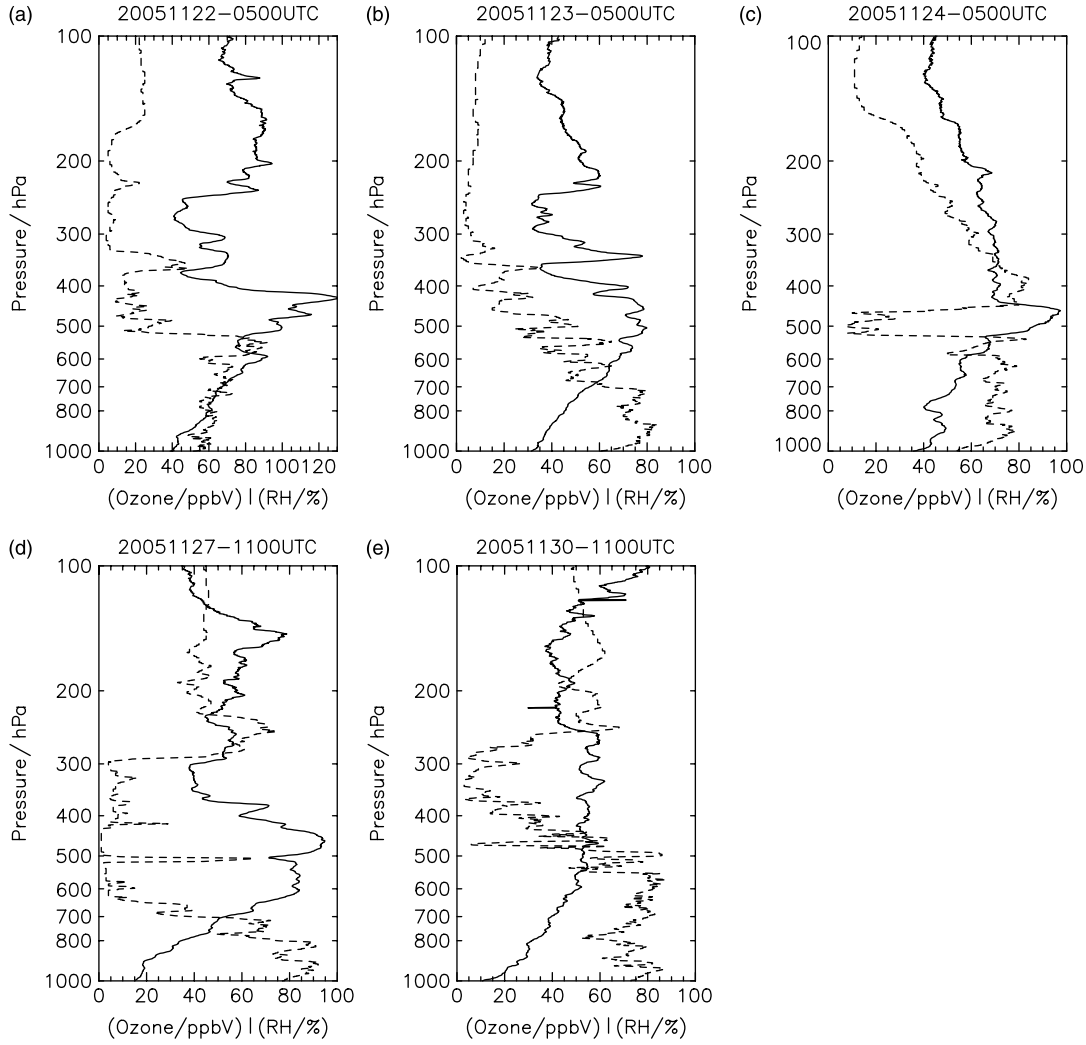

Figure 6. Vertical profiles of tropospheric ozone (solid line) concentration and relative humidity (dashed line) over water ($> 0\,^{\circ}$C) or over ice ($< 0\,^{\circ}$C) as appropriate, measured by ozonesondes launched from Darwin Airport between 22 and 30 November 2005 on the dates specified in each panel.

observed from the satellite – that is of most interest here, as it requires relatively little uplift of the boundary layer moist air to release the potential instability.

The most likely initiation mechanism over this coastal region during the dawn hours is convergence over the ocean due to land breezes. Such convergence is evident in winds derived from high spatial resolution Level 2 data (12.5 km) measured by the SeaWinds instrument on NASA's QuikSCAT satellite (described further by Dunbar et al., 2006) over the maritime area off the north-west coast of Australia (Figure 11). Unfortunately, there was no direct overpass of the coastal area where the cloud band was initiated on the morning of 20 November 2005 (the circle in Figure 11), despite there being direct overpasses on the previous and succeeding mornings and evenings. However, the QuikSCAT swath at this time did graze the area into which the cloud band extended twohours after its initiation, seen as the solid black line in Figure 11. The figure shows a very strong land breeze (up to 20 m s^{-1}) off the coast at 127°E, and a convergence of air at the point where convection was observed at the time of the QuikSCAT observation at 127°E, 12.5°S. Although direct measurements of the land breeze at the point of convective initiation are not available, we surmise that the observed land-breeze feature near 127°E extended eastward and that convergence at the land-breeze front is the likely mechanism for forced uplift to realize the potential instability generated by the low-level dry layers in Figure 10. Analysis of QuikSCAT data on previous and succeeding days (not shown here) shows similar, but weaker, convergence. Convective bands did not develop on these days, presumably due to the absence of potential instability.

The rapid development of convection along the line out to sea corresponds to a phase speed of approximately 40 m s^{-1} and thus suggests that convective development along the line was independent and not propagated by gust fronts. One possible explanation for this rapid development could be convectively generated gravity waves trapped in the boundary layer (which do have phase speeds similar to those required) such as that observed, for example, by Mapes (1993) in other organized tropical convective systems, and possibly providing the necessary uplift required to release the same potential instability

DOI: 10.1002/qj

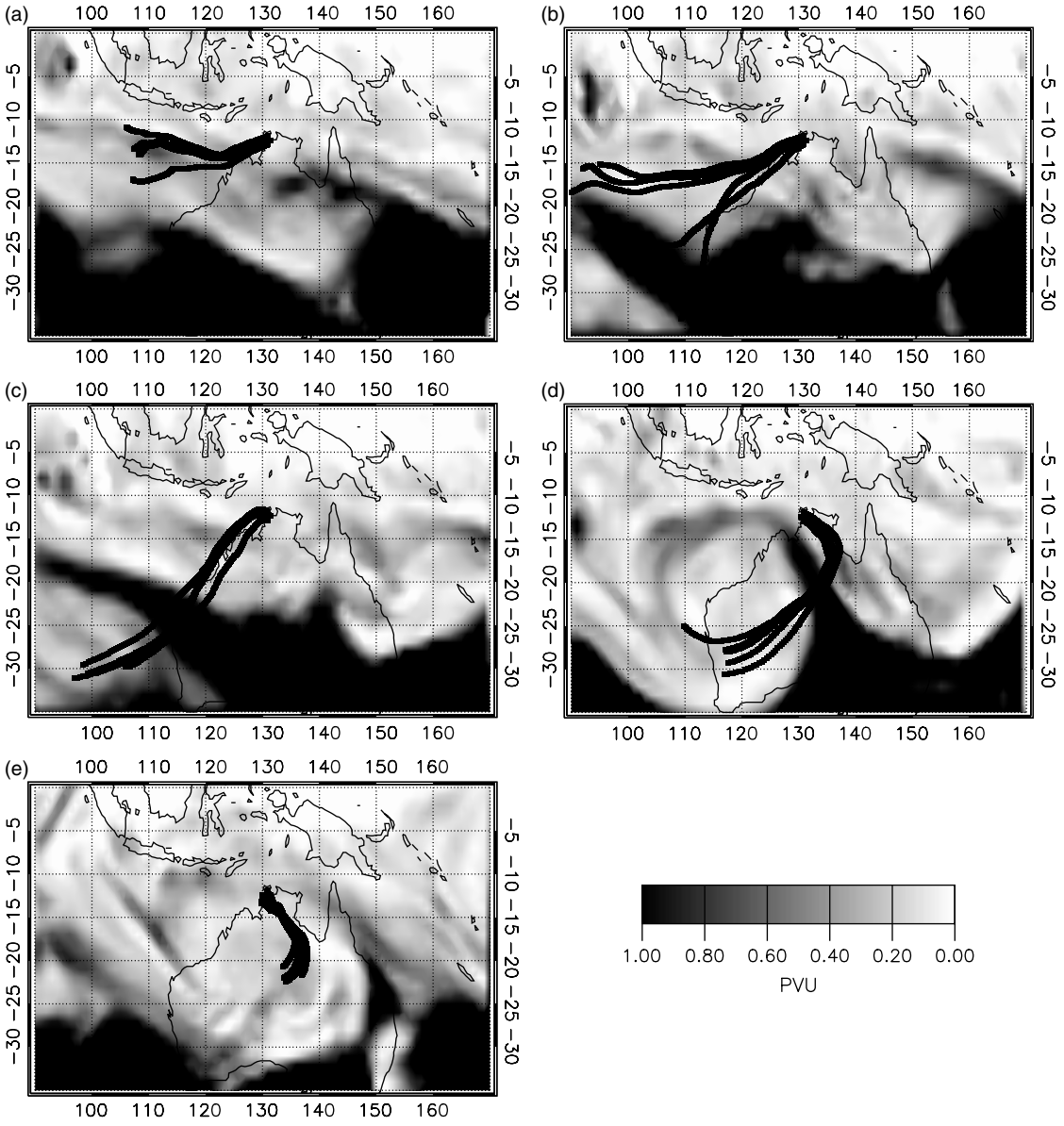

Figure 7. 0.5° clustered four-day ECMWF back trajectories corresponding to layers of enhanced ozone observed by ozonesondes (Figure 6) launched from Darwin, ending at 500 hPa centred on 130.9°E, 12.4°S, overplotted with ECMWF-derived PV fields at the isentropic surface at trajectory origin (indicated in each panel) for (a) 22 November 2005 0500 UTC, (b) 23 November 2005 0500 UTC, (c) 24 November 2005 0500 UTC, (d) 27 November 2005 1100 UTC and (e) 30 November 2005 1100 UTC.

over the ocean. However, a more likely explanation is the orientation of the dry slot with respect to the zone of convergence due to the land breeze observed in Figure 11; the land-breeze front is at a shallow angle to the dry–moist boundary, and so as the convergence zone intersected the boundary the convection would appear rapidly along this line. In summary, a synoptic-scale tropical cloud system developed along this line of potential instability at low levels. The origins of this feature are now investigated further.

5.2. Origins of the lower-level dry layer

Four-day back trajectories initiated from within the potentially unstable dry layer of reduced θ_w seen at around 900 mb in Figure 10 are plotted in Figure 12. A PV field derived from ECMWF analyses at 314 K is also plotted on the isentropic surface where the central trajectory terminated. These trajectories show that the dry layer originated from a breaking Rossby wave (the finger of high PV at the end of the trajectories in Figure 12. This event, on 16 November, preceded the Rossby wave breaking event of Figure 4 and was associated with the first of the dry periods in Figure 2. Thus, the tropopause fold emanating from this event was able to reach down to the top of the boundary layer by 26 November.

5.3. Discussion of tropical cloud band dynamics

Knippertz (2007) notes that there are a number of different views currently in the literature (see his section 5) concerning the relationship between convection and

DOI: 10.1002/qj

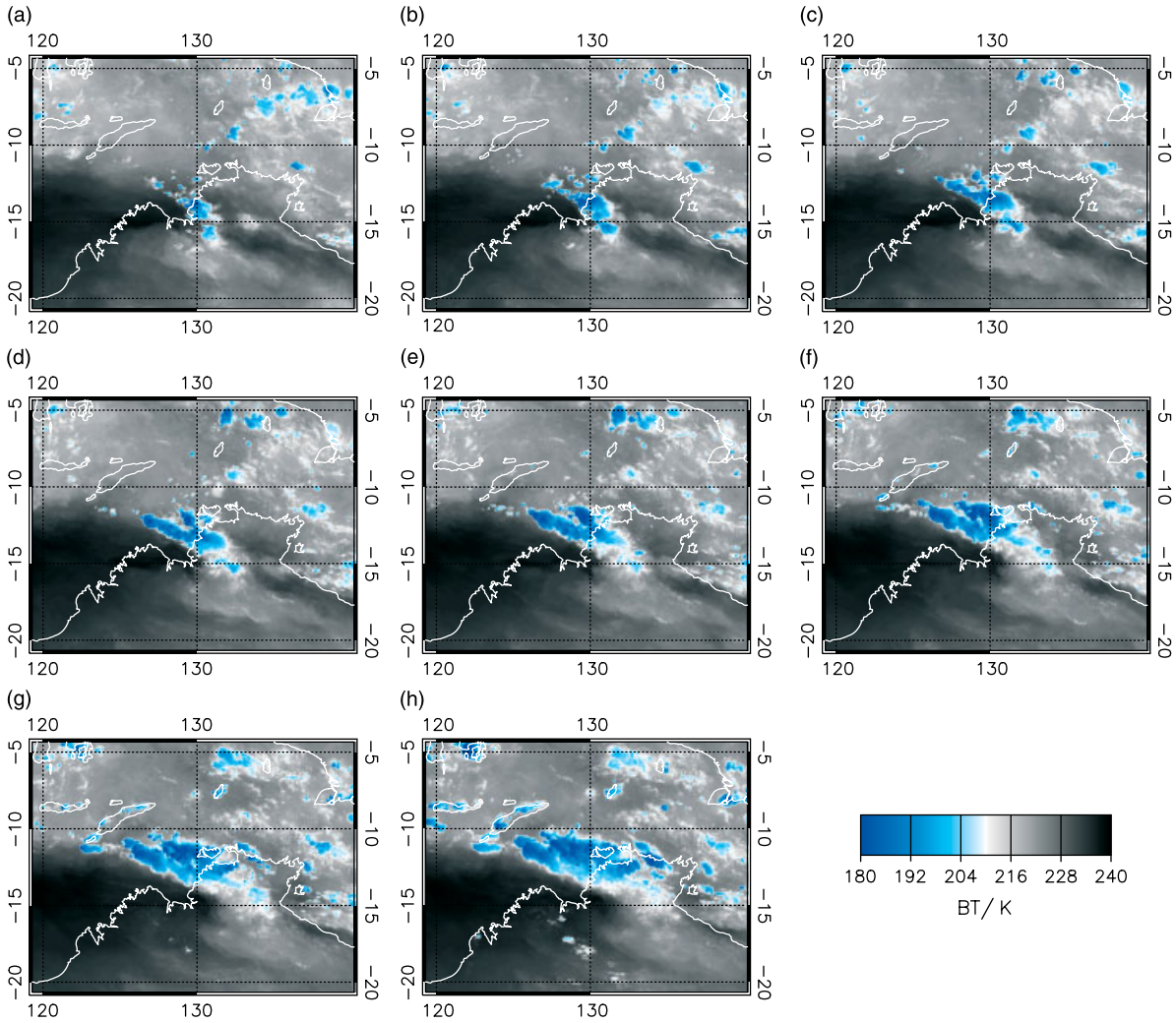

Figure 8. A sequence of MTSAT-1R water vapour channel false-colour images over northern Australia at one-hour intervals starting at 2226 UTC (0756 local +1 day) 19 November 2005 (upper left), showing the rapid development of a convective line near the boundary between moist (blue/white) and dry (brown/dark) air masses.

tropical plumes, and the existence of upper-level troughs; the key question is whether the observed lifting is a result of dynamical forcing, convective heating or some interaction between them. We suggest here that the tropical cloud band discussed in this study was not associated with an upper level trough due to the absence of any upper level PV signature near northern Australia at this time (Figure 4(a)), and formed as a result of the release (through land-breeze driven forcing) of potential instability generated in the lower troposphere by the advection of very dry air over the moist tropical boundary layer, as a result of the descent of air from tropopause levels caused by the Rossby wave breaking event of DP1.

6. Conclusions

Two tropical drought periods of reduced rainfall and cloud cover over tropical northern Australia were identified between 16–19 November 2005 and 23–27 November 2005 respectively. Both drought periods were found to coincide with the descent of dry upper tropospheric air advected from the midlatitudes in tropopause folds associated with a series of breaking Rossby waves observed on the southern STJ. In the second drought period a double Rossby wave breaking event facilitated the penetration of upper tropospheric midlatitude air well into the tropics over northern Australia as far north as 10°S; the first wave created a westerly wind duct for the latter to propagate further north. Fields from ECMWF analyses and back trajectories confirm that some at least of these layers originated in PV streamers of midlatitude origin generated by the Rossby waves. Satellite water-vapour imagery showed that a resultant dry pool resided over a large area of north-west Australia over both dry periods. In summary, despite the typically high tropical humidities of 70–80% recorded by radiosondes in the Darwin boundary layer (up to around 700 mb), the dry descending air measured at tropospheric mid-levels over Darwin inhibited deep convection for about five days over a wide area, except for coastal zones, where strong sea-breeze convergence was able to remove this convective inhibition.

In between the two dry periods and on the edge of the tropopause fold resulting from the first dry period,

DOI: 10.1002/qj

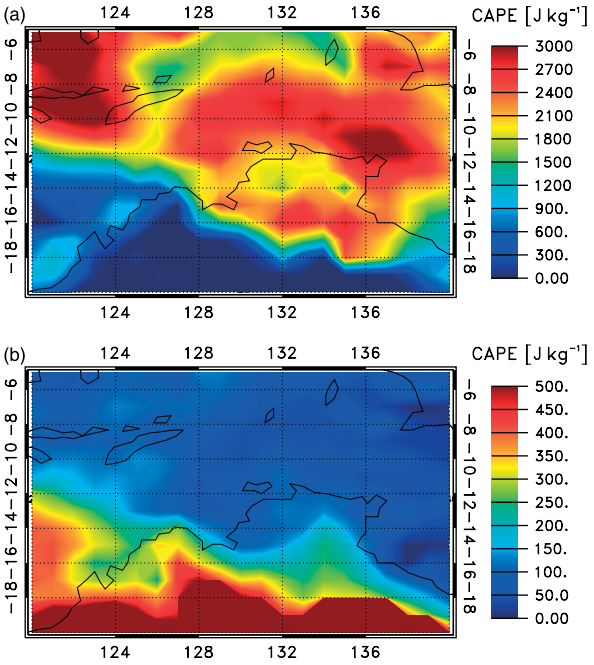

Figure 9. Contours of (a) convective available potential energy (CAPE); and (b) convective inhibition (CIN) over tropical northern Australia at 0000 UTC on 20 November 2005, diagnosed from ECMWF analysis thermodynamic fields.

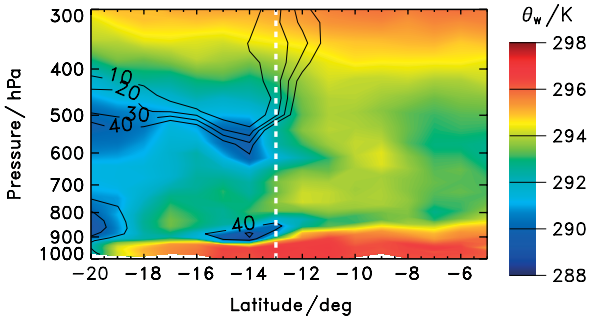

Figure 10. A cross-section in latitude of wet-bulb potential temperature (colour contours) derived from ECMWF analysis fields through the 129°E meridian at 0000 UTC (0930 local time) on 22 November 2005. Labelled black contours define relative humidity isopleths. The dashed white line highlights 14°S.

a tropical cloud band was observed to form rapidly on 20 November 2005 near to a sharp boundary between moist and dry air in satellite water vapour images. This convection was initiated off the north-west coast of Australia at 0730 local time (2200 UTC on previous day) on 20 November. The rapid development (six hours) of this cloud structure was associated with the forced release of potential instability generated as dry air overrode moist air in the continental and maritime boundary layers. The forcing required to release this instability is consistent with the convergence of strong land breezes off the coastal region, as seen by QuikSCAT in the region to the west.

We therefore conclude that breaking Rossby waves along the STJ can affect tropical convection in two main ways.

(1) As the waves break they introduce into the tropical troposphere descending layers of very dry, ozone-rich air. In some cases these have high potential vorticity, which manifests itself as high static stability, providing convective inhibition. In other cases the signature is purely one of composition, and the suppression of convection must then be due to entrainment of dry air into rising convective plumes.

(2) At the leading edges of the descending dry air, and where sufficient low-level forcing is present, potential instability can be released, leading to plumes of deep tropical convection.

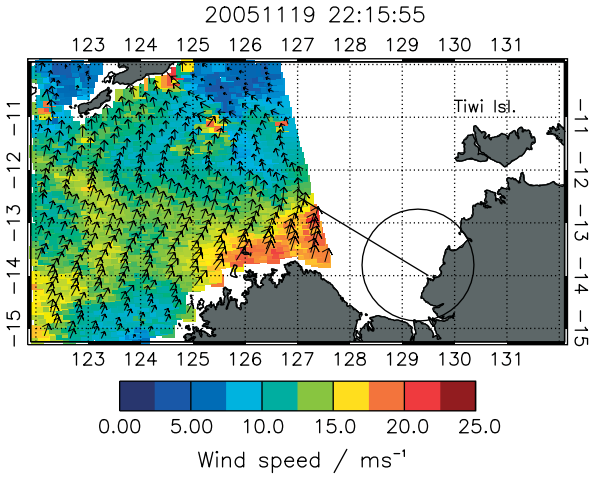

Figure 11. Sea-level wind speed (colour contours) and direction (scaled black arrows) off the west coast of northern Australia as measured by QuikSCAT (12.5 km horizontal resolution) at 2215 UTC (0745 local time) on 20 November 2005. The circle illustrates the area where convection was initiated, as observed in MTSAT images at 0650 local time. The line illustrates the extent of the cloud band at the time of the QuikSCAT measurement.

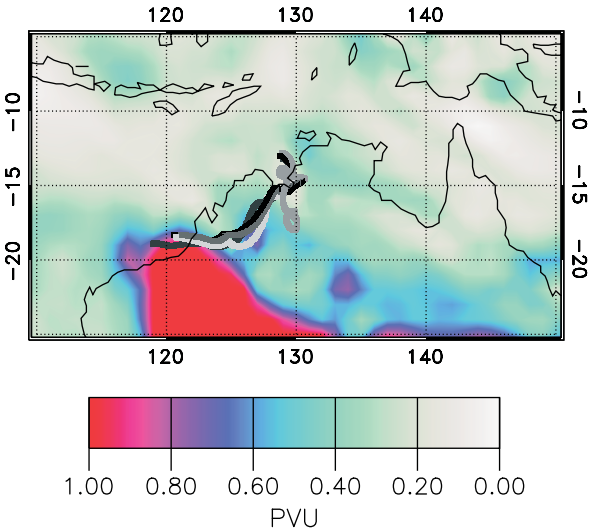

Figure 12. 0.5° clustered four-day ECMWF back trajectories originating at 0000 UTC on 20 November 2005, corresponding to the layer of potential instability at 900 mb (Figure 11) centred at 129°E, 14°S. ECMWF-derived PV fields (colour contours) are overplotted on the 314 K isentropic surface at trajectory origin.

DOI: 10.1002/qj

The frequency of tropopause fold events and their potentially important impact on tropical convection, as demonstrated here, is currently poorly characterized. These observations support a growing number of studies linking midlatitude dynamics with the modulation of tropical deep convection and highlight the need for such processes to be considered in studies of tropical deep convective processes and tropical tropospheric chemistry and composition.

Acknowledgements

The ACTIVE campaign was funded by a Natural Environment Research Council consortium grant (NE/C512688). European Centre for Medium-Range Weather Forecasts (ECMWF) Operational Analysis data were provided by the British Atmospheric Data Centre. Available from: http://badc.nerc.ac.uk/data/ecmwf-op/. Support for the MTSAT-1R analyses was provided by the Department of Energy ARM Program.

References

Bithell M, Vaughan G, Gray LJ. 2000. Persistence of stratospheric ozone layers in the troposphere. *Atmos. Environ.* **34**: 2563–2570.

Browning KA, Roberts NM. 1994. Use of satellite imagery to diagnose events leading to frontal thunderstorms, Part 1. *Meteorol. Appl.* **1**: 303–310.

Browning KA, Roberts NM. 1995. Use of satellite imagery to diagnose events leading to frontal thunderstorms, Part 2. *Meteorol. Appsl.* **2**: 3–9.

Brunner D, Siegmund P, May PT, Chappel L, Schiller C, Muller R, Peter T, Fueglistaler S, Mackenzie AR, Fix A, Schlager H, Allen G, Fjaeraa AM, Streibel M, Harris NRP. 2008. The SCOUT-O3 Darwin Aircraft Campaign: rationale and meteorology. *Atmos. Chem. Phys. Discuss.* **8**: 17131–17191.

Cau P, Methven J, Hoskins B. 2005. Representation of dry tropical layers and their origins in ERA-40 data. *J. Geophys. Res.* **110**: D06110, DOI:10.1029/2004JD004928.

Danielsen EF. 1968. Stratospheric–tropospheric exchange based on radioactivity, ozone, and potential vorticity. *(J. Atmos. Sci.)* **25**: 502–518.

Davidson NE, Tory KJ, Reeder MJ, Drosdowsky WL. 2007. Extratropical–tropical interaction during onset of the Australian monsoon: reanalysis diagnostics and idealized dry simulations. *J. Atmos. Sci.* **64**: 3475–3498.

Dunbar RS, Lungu T, Weiss B, Stiles B, Huddleston J, Callahan PS, Shirtliffe G, Perry KL, Hsu C, Mears C, Wentz F, Smith D. 2006. QuikSCAT Science Data Product User's Manual, Version 3.0, JPL Document D-18053-Rev A. Jet Propulsion Laboratory: Pasadena, CA.

Forster C, Wirth V. 2000. Radiative decay of idealized stratospheric filaments in the troposphere. *J. Geophys. Res.* **105**(D8): 10169–10184.

Hoskins BJ, Ambrizzi T. 1993. Rossby wave propagation on a realistic longitudinally varying flow. *J. Atmos. Sci.* **50**: 1661–1671.

Kiladis GN. 1998. Observations of Rossby waves linked to convection over the eastern tropical Pacific. *J. Atmos. Sci.* **55**: 321–339.

Knippertz P. 2005. Tropical-extratropical interactions associated with an Atlantic tropical plume and subtropical jet streak. *Mon. Weather Rev.* **133**: 2759–2776.

Knippertz P. 2007. Tropical-extratropical interactions related to upper-level troughs at low latitudes. *Dyn. Atmos. Oceans* **43**: 36–62.

Knippertz P, Martin JE. 2006. The role of dynamic and diabatic processes in the generation of cut-off lows over northwest Africa. *Meteorol. Atmos. Phys.* **96**: 3–19. DOI:10.1007/s00703-006-0217-4.

Mapes BE. 1993. Gregarious tropical convection. *J. Atmos. Sci.* **50**: 2026–2037. DOI:10.1175/1520-0469.

Mapes BE, Zuidema P. 1996. Radiative-dynamical consequences of dry tongues in the tropical troposphere. *J. Atmos. Sci.* **53**: 620–638.

Minnis P, Young DF, Kratz DP, Coakley JA Jr., King MD, Garber DP, Heck PW, Mayor S, Arduini RF. 1995. Cloud Optical Property Retrieval (Subsystem 4.3). *Clouds and the Earth's Radiant Energy System (CERES) algorithm theoretical basis document, Volume III: cloud analyses and radiance inversions (Subsystem 4), NASA RP 1376*, CERES Science Team (eds). NASA. Pp. 135–176.

Minnis P, Nguyen L, Smith WL, Palikonka R, Ayers JK, Doelling DR, Nordeen ML, Spangenberg D, Phan DN, Khaiyer M, Mace GG. 2006. Large-scale cloud properties and radiative fluxes over Darwin during TWP-ICE. *Proc. 16th ARM Sci. Team Mtg., Albuquerque, NM, March 27-31.* (http://www.arm.gov/publications/proceedings/conf16/extended_abs/minnis_p.pdf).

Morcrette C, Humphrey L, Browning KA, Nicol J, Roberts N, Clark P, Russell A, Blyth A. 2007. Combination of mesoscale and synoptic mechanisms for triggering an isolated thunderstorm: observational case study of CSIP IOP 1. *Mon. Weather Rev.* **135**: 3728–3749.

Parsons DB. 1999. Recovery processes and factors limiting cloud-top height following the arrival of a dry intrusion observed during TOGA COARE. *J. Atmos. Sci.* **59**: 2438.

Parsons DB, Yoneyama K, Redelsperger J-L. 2000. The evolution of the tropical western Pacific atmosphere–ocean system following the arrival of a dry intrusion. *Q. J. R. Meteorol. Soc.* **126**: 517–548.

Reid SJ, Vaughan G, Marsh ARW, Smith SJ. 1996. Accuracy of ozonesonde measurements in the troposphere. *J. Atmos. Chem.* **25**: 215–226.

Roca R, Lafore J-P, Piriou C, Redelsperger J-L. 2005. Extratropical dry-air instrusions into the west African monsoon midtroposphere: an important factor for the convective activity over the Sahel. *J. Atmos. Sci* **62**: 390–407.

Slingo JM, 1998. Extratropical forcing of tropical convection in a northern winter simulation with the UGAMP GCM. *Q. J. R. Meteorol. Soc.* **124**: 27–51.

Sprenger M, Maspoli MC, Wernli H. 2003. Tropopause folds and cross-tropopause exchange: a global investigation based upon ECMWF analyses for the time period March 2000 to February 2001. *J. Geophys. Res.* **108**: D8518, DOI:10.1029/2002JD002587.

Vaughan G, Schiller C, MacKenzie AR, Bower K, Peter T, Schlager H, Harris NRP, May PT. 2008. SCOUT-O3/ACTIVE: high-altitude aircraft measurements around deep tropical convection. *Bull. Am. Meteorol. Soc.* **89**: 5, DOI: 10.1175/BAMS-89-5-647.

Yoneyama K, Parsons DB. 1999. A proposed mechanism for the intrusion of dry air into the Tropical Western Pacific region. *J. Atmos. Sci.* **56**: 1524–1546.